Polymer Journal
https://doi.org/10.1038/s41428-024-00957-y

ORIGINAL ARTICLE

High-strength, conductive, double-network self-healing antibacterial hydrogel based on the coordination bond and dynamic imine bond

Yalei Liu[1] · Junfang Chang[2] · Zhiyong Guo[2] · Sui Wang[2] · Jie Mao[3]

Received: 23 June 2024 / Revised: 1 August 2024 / Accepted: 2 August 2024

Abstract

Multifunctional hydrogel materials are being increasingly used in wearable sensing devices and biomedical applications, but the comprehensive performance of hydrogel materials must be further developed. To prepare hydrogels with better self-healing properties, biomacromolecules such as sodium alginate and carboxymethyl chitosan were used as raw materials by combining the dynamic imine bonding network formed by both materials with the coordination bonding network formed by acrylic acid and aluminum ions. The double network structure of the hydrogel provides the hydrogel with excellent self-healing properties (up to 127% recovery of toughness after self-healing) and good mechanical properties with a fracture strain of 3787%. Substances with antimicrobial properties in the hydrogel network inhibited the growth of *E. coli* and *S. aureus*. In addition, the hydrogel has good electrical conductivity with a conductivity of 1.41 S/m. This study examined multiple properties of the hydrogel and provides a reference for the application of this material in practical application scenarios.

Introduction

Hydrogels are a class of soft and wet materials with a three-dimensional network structure and adjustable physical and chemical properties due to their structural peculiarities [1]. Currently, hydrogels have been studied in terms of self-healing properties [2], antimicrobial properties [3], conductive properties [4], photosensitivity [5], structural variability [6], and programmability [7]. The applications of hydrogels are mainly in food monitoring [8], green coatings [9], biosensing [10], medical wound dressings [11], drug delivery [12] and regenerative tissue engineering [13]. In recent years, researchers have attempted to improve the properties of hydrogels starting from practical application scenarios, so research on multifunctional hydrogels has increased.

Self-healing hydrogels are a class of hydrogel materials with autonomous recovery ability that can repair themselves and restore their relevant properties after damage. The self-healing properties of hydrogels are similar to the self-healing properties of living organisms. Coupled with the recent trend of hydrogels in biomedical applications, many researchers have attempted to use self-healing hydrogels as wound dressings. Yang et al. [14] used dopamine-functionalized oxidized hyaluronic acid (OHA-Dop), adipic dihydrazide-modified HA (HA-ADH), and aldehyde-capped Pluronic F127 (AF127) as a polymer backbone to develop an injectable micellar hydrogel (AF127/HA-ADH/OHA-Dop) with excellent adhesion and self-healing properties that accelerated skin wound healing. He et al. [15] developed a series of injectable pH-responsive self-healing hydrogel adhesives based on acryloyl-6-aminohexanoic acid (AA) and AA-gN-hydroxysuccinimide (AA-NHS) with hemostatic and wound-healing properties as endoscopic spray bioadhesive materials.

Supplementary information The online version contains supplementary material available at https://doi.org/10.1038/s41428-024-00957-y.

✉ Sui Wang
wangsui311@163.com

[1] Department of Agricultural Economics and Management, Zhejiang Agricultural Business College, Shaoxing 312000, People's Republic of China

[2] State Key Laboratory for Managing Biotic and Chemical Threats to the Quality and Safety of Agro-products, State Key Laboratory Base of Novel Functional Materials and Preparation Science, School of Materials Science and Chemical Engineering, Ningbo University, Ningbo 315211, People's Republic of China

[3] Department of Basic, Zhejiang Pharmaceutical University, Ningbo, China

Published online: 03 September 2024

In biomedical applications, the applicability of hydrogel materials with only self-healing properties is not sufficient; thus, some researchers are preparing self-healing hydrogel materials with multiple properties. Chen et al. [16] designed hydrogels with self-healing, adhesive and antibacterial properties based on gelatin methacrylate (GelMA), adenine acrylate (AA), and $CuCl_2$ to promote diabetic wound healing. Yang et al. [17] prepared a hybrid hydrogel dressing that consisted of a simple copolymer of acrylamide (AM), 3-acrylamidophenylboronic acid (AAPBA), chitosan (CS), and a nanoscale tannic acid (TA)/ferric ion (Fe^{3+}) complex (TFe). The resulting hydrogel exhibited good mechanical properties, rapid self-healing ability, and good tissue repair ability. Inspired by the concept of moist wound healing, Deng et al. [18] prepared an injectable hydrogel material with antimicrobial properties and self-healing properties to accelerate wound healing.

Antimicrobial properties are often essential in wound dressings because of the susceptibility of wounds to bacterial infections. In addition, wearable sensing devices are now often required to have certain antimicrobial properties. Liu et al. [19] prepared conductive dual-network hydrogels (ACBt-PAA/CMCs) from carboxymethyl chitosan (CMCs), acrylic acid (AA), and alkaline calcium bentonite (ACBt) using a facile method with excellent sensing and self-adhesive properties; these hydrogels exhibited excellent real-time sensing performance as wearable devices to monitor various motions. Wang et al. [20] developed a bilayer-structured flexible wearable sensor based on a conductive composite hydrogel with an outer layer of silicone elastomer (Ecoflex)/silica particle composite film and an inner layer of P(AAm-co-HEMA)-MXene-AgNP hydrogel, which combined superhydrophobic, conductive, antibacterial and self-adhesive functions to monitor human activities and joint movements. Hydrogels that combine self-healing, antibacterial, and electrical conductivity properties have great potential for development in biomedical fields such as wound dressings and in the application of wearable smart sensing devices. However, since the current polymer materials to prepare hydrogels cannot simultaneously combine many properties, the current trend is to prepare hydrogels with multiple functions by combining multiple substances as needed.

In this work, to make hydrogels with excellent self-healing properties, we combined the coordination of acrylic acid (AA) and Al^{3+} with the dynamic imine bonding of sodium-oxidized alginate (OSA) and carboxymethyl chitosan (CMCS) to prepare PAA/CMCS/OSA/Al^{3+} hydrogels with excellent mechanical properties, self-healing properties, antibacterial properties, and electrical conductivity. The double network structure of this hydrogel confers good self-healing properties and mechanical properties to the hydrogel. The hydrogel also inhibited the growth of *E. coli* and *S. aureus* because there were substances with antibacterial properties such as Al^{3+}, CMCS, and OSA in the hydrogel network. In addition, the hydrogel exhibited excellent electrical conductivity. This study considers multiple properties of hydrogels and provides a reference for the application of hydrogel materials in more practical application scenarios.

Materials and methods

Materials

Acrylic acid, carboxymethyl chitosan (CMCS, 80% carboxylation), sodium alginate (SA), sodium periodate, ethylene glycol, sodium chloride, aluminum chloride hexahydrate ($AlCl_3{\cdot}6H_2O$), ammonium persulfate, anhydrous ethanol, TSB medium, LB solid medium and deionized water were used. All other chemicals and deionized water in this experiment were of analytical grade.

Methods

Preparation of sodium alginate oxide

The preparation of sodium alginate oxide was described in a previous report [21]. One gram of sodium alginate was added to 100 mL of water and stirred in a water bath at 45°C for 2 h. After sodium alginate was completely dissolved, 0.268 g of sodium periodate was added, and the mixture was stirred at room temperature for 4 h. After its oxidation was complete, 1 mL of ethylene glycol was added, and the mixture was left for 2 h in the dark. Then, 0.3 g of sodium chloride was added, the mixture was stirred to dissolve, and 200 mL of anhydrous ethanol was added to precipitate a white suspension. After filtering, cleaning, freeze-drying and grinding, the oxidized sodium alginate powder was obtained. The hydroxylamine hydrochloride titration method was used to determine the aldehyde content in the OSA. This method is based on the principle that the aldehyde group reacts with the amino group in hydroxylamine hydrochloride to form an oxime and hydrochloric acid (HCl), and the amount of aldehyde group in OSA is calculated by titrating the amount of HCl with a sodium hydroxide solution [22]. Briefly, lyophilized OSA (0.10 g) was dissolved in a hydroxylamine hydrochloride solution (0.25 M, 25 mL). A chromogenic indicator (methyl orange, 0.05% solution, 100 µL) was added and left for 2 h. The solution was titrated with NaOH (0.1 M); at the end of the titration, the color of the solution changed from pink to yellow, and the NaOH consumption was recorded [23]. The aldehyde substitution of OSA was determined as follows:

$$\mathrm{AC}(\%) = \frac{198 \times V \times c \times 10^{-3}}{2 \times W} \times 100\%$$

where V is the volume of NaOH solution consumed (mL); c is the concentration of NaOH solution (mol·L^{-1}); W is the mass of OSA (g); 198 is the molecular weight of the OSA repeating unit (g·mol^{-1}).

Preparation of the PAA/CMCS/OSA/Al^{3+} hydrogel

One gram of solid $AlCl_3$•$6H_2O$ was added to 20 mL of deionized water, stirred, and dissolved; then, 6 mL of acrylic acid, CMCS (0.3 g), or OSA (0.3 g) was added. The mixed solution was stirred well in a water bath at 60°C and subsequently stirred at room temperature. After the temperature was lowered to room temperature, 0.1 g of ammonium persulfate was added to the solution and stirred well; then, the mixed solution was transferred to a mold and heated in a water bath at 60°C for 1 h. The PAA/CMCS/OSA/Al^{3+} hydrogel was formed and recorded as an H-1 sample in this work. To investigate the effects of different components on this hydrogel, this study investigated the effects of dibasic Al^{3+}, CMCS, and OSA contents on the hydrogel properties of H-1 samples, which were denoted as H-2, H-3, and H-4 samples, respectively.

Analytical characterization of the PAA/CMCS/OSA/Al^{3+} hydrogel

NMR and Infrared characterization of sodium oxide alginate (OSA)

In this study, the synthesized sodium alginate oxide was characterized via FTIR (Nicolet-6700; USA) and Bruker 400 M instruments. For infrared testing, the samples were ground and pressed into tablets with potassium bromide. The scanning resolution was 4 cm^{-1}. For NMR testing, the samples were dissolved in deuterium water. All tests were performed in triplicates.

FTIR spectral characterization of the materials

The PAA, CMCS, OSA, and PAA/CMCS/OSA/Al^{3+} hydrogel materials were separately characterized by FTIR spectroscopy (Nicolet-6700; USA). Among the tested parameters, the spectral scanning range was from 4000 cm^{-1} to 500 $cm^{-1,}$ with a scanning resolution of 4 cm^{-1}.

Scanning electron microscopy (SEM) analysis of the materials

The hydrogels with different substance contents were lyophilized under vacuum and then sprayed with gold. The morphology of the hydrogels was observed and analyzed by scanning electron microscopy (Nova Nano SEM 450; USA).

Characterization of hydrogel mechanical properties

The mechanical properties of the hydrogels were tested using a universal testing machine model WH-5000. The samples were cylindrical in shape (4 mm in diameter and 12 mm in length). The test rate was set at 30 mm·min^{-1}. The fracture stress (σ) is the ratio of the loading force (F) to the initial cross-sectional area (A). The strain at break (ε) is the ratio of the length (l) of the hydrogel sample at break to the initial length (l_0) of the hydrogel sample.

Investigating the self-healing properties of hydrogels

The hydrogel was physically divided into two halves, one of which was stained and the other was unstained. Then, the two halves were placed in contact for 20 min at room temperature to observe the self-healing results of the hydrogel. Another method involves observing the morphology of the healed hydrogel using sweeping electron microscopy.

Rheological characterization of the hydrogels

The hydrogels were made into shapes that were 2 mm thick and 20 mm in diameter for rheological property testing. First, the hydrogels were subjected to strain scanning tests (γ, 0.01%–100%). Then, the hydrogels before and after self-healing were subjected to alternating strain scanning tests of 1% (100 s) and 10% (100 s), respectively. The entire test was performed at a controlled test temperature of 25°C and a frequency of 1 Hz. Three sets of parallel experiments were repeated using a rotational rheometer (HAAKE MARS; GER).

Electrical conductivity study

The conductive and sensing properties of the hydrogels were tested using an electrochemical station (CHI 660E). The conductive properties of the hydrogels were recorded by an electrochemical system at a constant voltage of 1 V. The conductivity of the hydrogel was measured with a two-point probe, and the equation for the conductivity of the hydrogel can be obtained as follows:

$$\sigma = \frac{IL}{U\pi r^2}$$

where σ (S/m) is the electrical conductivity of the hydrogel; L (cm) and r (cm) are the length and diameter of the hydrogel, respectively.

The sensing performance of the hydrogel was characterized by the change in relative resistance, and the relative resistance $\triangle R/R_0$ is:

$$\triangle R/R_0 = (R - R_0)/R_0$$

where R_0 (Ω) and R (Ω) are the resistance without strain and resistance with strain, respectively.

Testing the antimicrobial properties of the hydrogels

In this study, the inhibitory effects of the hydrogels against *S. aureus* and *E. coli* were separately tested. The testing method was performed according to the literature [24]. First, the antimicrobial effects of the hydrogels were visualized using the ring-of-inhibition method. The hydrogel samples were placed on medium plates at the corresponding concentrations, and the formation of an inhibition circle around the hydrogel was observed.

Another method was plate counting. First, 0.12 g of hydrogel and 60 μL of bacterial suspension (OD600 = 1.0) were placed in sterile test tubes and co-cultured at 37 °C for 1.5 h. After 1.5 h, 940 μL of sterile medium was added to each sterile test tube. The blank control group was incubated under identical conditions with 60 μL of bacterial suspension that did not contact the hydrogel samples. Finally, 100 μL of the above suspension was inoculated onto agar plates, incubated at 37 °C for 24 h in an incubator, and removed for counting. Three media plates were coated for each concentration. Because of the large concentration in the test experiment, the blank sample group could not be counted; therefore, in this experiment, only the antibacterial performance of the hydrogel was determined from a macroscopic viewpoint and not considered.

To demonstrate the antibacterial properties of the hydrogel from multiple perspectives, the growth inhibition process of *E. coli* and *S. aureus* by this hydrogel was observed via OD600 monitoring [25]. First, 0.5 g of hydrogel was weighed and packed into sterile centrifuge tubes. Then, the weighed hydrogels were sterilized under UV light for half an hour. The OD600 value of the bacterial suspension was adjusted to approximately 0.5. Next, the prepared bacterial suspensions were added to centrifuge tubes corresponding to the hydrogel numbers, and no hydrogel samples were added to the blank group. The co-cultured bacterial suspensions were incubated at 37 °C in an incubator, and a certain amount of bacterial suspensions was taken every hour in an enzyme marker plate; their corresponding OD values were measured using an enzyme marker (TECAN; Switzerland), and each value was measured three times and averaged.

Results and discussion

Characterization of sodium alginate oxide

Oxidized sodium alginate (OSA), which contains aldehyde groups, is the product of the oxidation of sodium alginate (SA) by sodium periodate. The successful preparation of the structure was confirmed by NMR and IR tests. The left panel of Fig. S1 shows its 1H NMR spectrum; the peak at 8.34 ppm is attributed to the aldehyde proton of the aldehyde moiety [23], and two proton peaks at 5.38 and 5.61 ppm are attributed to the hemiacetal proton formed by the aldehyde and adjacent hydroxyl group [26, 27]. From the IR spectra of OSA and SA in the right panel of the figure, the new peak at 1733 cm^{-1} for OSA is its characteristic aldehyde peak compared with that of SA [23, 26]. Moreover, the aldehyde substitution degree of OSA was determined to be 37.62% according to the hydroxylamine hydrochloride titration method. All results indicate the successful synthesis of OSA.

Preparation of the PAA/CMCS/OSA/Al^{3+} hydrogel

Figure 1 shows a schematic diagram of the PAA/CMCS/OSA/Al^{3+} hydrogel synthesis. Acrylic acid is a carboxyl-rich compound, and its abundant carboxyl groups can form coordination bonds with Al^{3+} in the system [28]. Carboxymethyl chitosan (CMCS), which contains amino and carboxyl groups, has been widely used in recent years to prepare trauma-based biomaterials and tissue engineering matrix materials because of its good biocompatibility and biodegradability [29]. The sodium oxide alginate (OSA) synthesized in this study contains an aldehyde group that forms a dynamic imine bond with the amino group in CMCS. In this study, the ligand bonding of acrylic acid with Al^{3+} and the dynamic imine bonding of carboxymethyl chitosan with sodium alginate oxide constitute the hydrogel system.

In this hydrogel system, the coordination interaction between PAA and Al^{3+} and the dynamic imine bonding between CMCS and OSA are the keys to achieving the self-healing properties of the hydrogel. The strong interaction between the carboxyl groups in PAA and Al^{3+} endows the hydrogel system with excellent mechanical properties. The introduction of OSA or Al^{3+} endows the PAA/CMCS/OSA/Al^{3+} hydrogel with good electrical conductivity. The introduction of CMCS and OSA dynamic imine bonding networks improves the tensile strength of hydrogels and enhances the self-healing properties of hydrogels.

Structure of the PAA/CMCS/OSA/Al^{3+} hydrogel

To understand the interactions of AA, Al^{3+}, OSA, and CMCS, the PAA/CMCS/OSA/Al^{3+} hydrogels and their raw materials were characterized via FTIR spectroscopy. As shown in Fig. 2, an absorption peak at 3400–3600 cm^{-1} was observed in all spectrograms, which was attributed to the stretching vibration of O–H [30]. After the addition of Al^{3+} to the hydrogel system, the stretching vibration peak of the

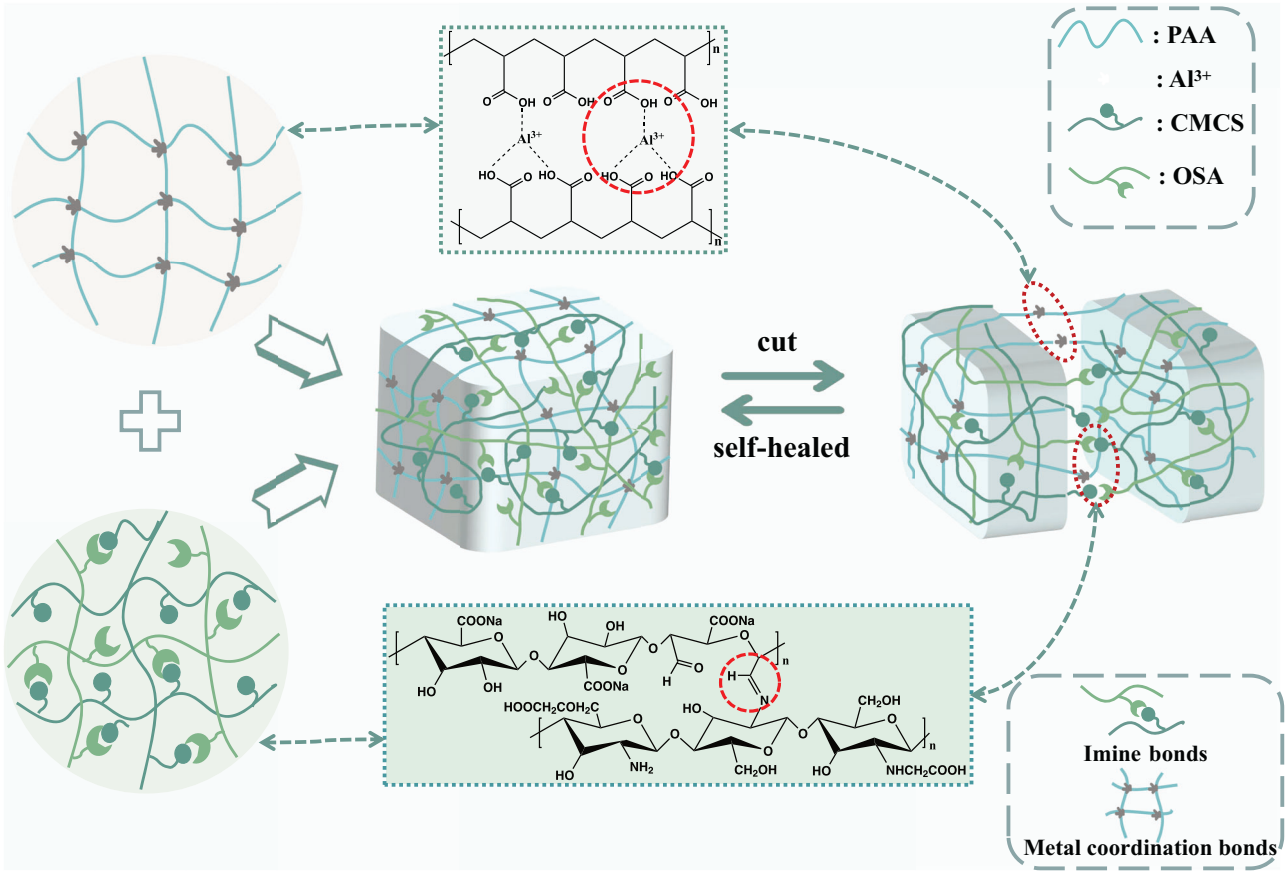

Fig. 1 Schematic diagram of the synthesis of the PAA/CMCS/OSA/Al^{3+} hydrogel

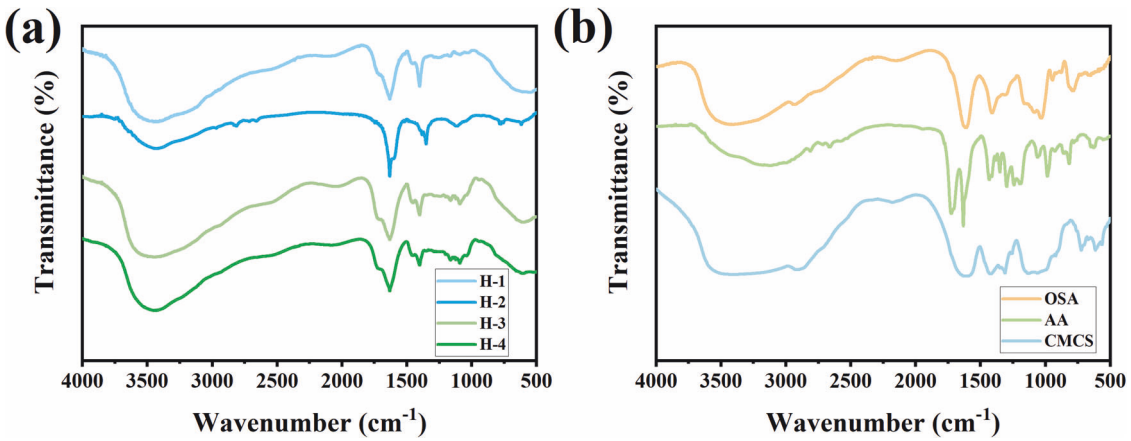

Fig. 2 Infrared spectra of (**a**) PAA/CMCS/OSA/Al^{3+} hydrogels with different ratios and (**b**) OSA, AA, and CMCS

C = O group at 1715 cm^{-1} in the AA sample did not shift, but its intensity gradually weakened [28]. The characteristic peak at 1635 cm^{-1} in the PAA/CMCS/OSA/Al^{3+} hydrogel sample is attributed to the characteristic peak of ionized carboxyl stretching asymmetric vibrations, which indicates the formation of coordination bonds [24, 28]. The C = N stretching vibrational peak of the imine bond is commonly at 1615–1660 cm^{-1} [31, 32], which has a similar conjugation effect as the C = O and C = C groups. Thus, the C = N stretching vibration of the imine bond overlaps with the characteristic peak of the coordination bond in the PAA/CMCS/OSA/Al^{3+} hydrogel spectrogram [23]. The characteristic peaks of the symmetric vibration of the aldehyde group (C = O) at 1733 cm^{-1} for OSA and the characteristic peak of the bending vibration of the amino group (-NH_2) at 1597 cm^{-1} for CMCS [33] completely

disappeared in the spectrograms of the hydrogel samples. A strong and distinct new peak at 1633 cm^{-1} appeared in the PAA/CMCS/OSA/Al^{3+} hydrogel spectrogram. This result verifies the formation of dynamic imine bonds between OSA and CMCS [34].

Morphological analysis of the PAA/CMCS/OSA/Al^{3+} hydrogel

To investigate the structure and morphology of the PAA/CMCS/OSA/Al^{3+} hydrogels, the morphologies of the hydrogels with different components were characterized by scanning electron microscopy, as shown in Fig. 3. Figure 3a shows that the pure PAA/Al^{3+} hydrogel at the same scale had a porous three-dimensional network structure with non-uniform pore sizes and thin pore walls. Figure 3b shows a scanning electron micrograph of the OSA/CMCS hydrogel at the same scale, where the morphology of the hydrogel was fragmented, and there were poor cross-linking and thin and nonuniform pore walls. Figure 3c–f show the morphology of the PAA/CMCS/OSA/Al^{3+} hydrogels with different ratios. The hydrogels had a dense structure after the combination of two networks, the pore size of the hydrogels decreased, and the pore wall became thicker with increasing Al^{3+}. With increasing CMCS/OSA network density, the porous structure of the hydrogel gradually disappeared, which indicates that the hydrogel structure became more rigid, and this result is consistent with the mechanical properties of the hydrogel.

Analysis of the mechanical properties of the PAA/CMCS/OSA/Al^{3+} hydrogel

Figure 4 shows the excellent mechanical tensile properties of PAA/CMCS/OSA/Al^{3+}. The maximum tensile stress of this hydrogel can reach 98 KPa, the strain at break can reach 3787%, and the toughness can reach 1.7 MJ/m^3 according to a universal tensile machine test. The data in the figure show that the hydrogel has good tensile strength and excellent fracture strain. With increasing Al^{3+} content, both tensile strength and fracture strain tended to decrease, which is consistent with previous reports [28]. With increasing CMCS and OSA contents, the tensile strength of the hydrogels significantly increased. This behavior can be attributed to the introduction of the imine bond network, which led to tighter connections among the hydrogel networks. The excellent mechanical tensile properties of the PAA/CMCS/OSA/Al^{3+} hydrogel provide more possibilities for the application of hydrogels in practical scenarios.

To test the self-recovery performance of the PAA/CMCS/OSA/Al^{3+} hydrogel, continuous load-unload cycle tests were conducted on the PAA/CMCS/OSA/Al^{3+}

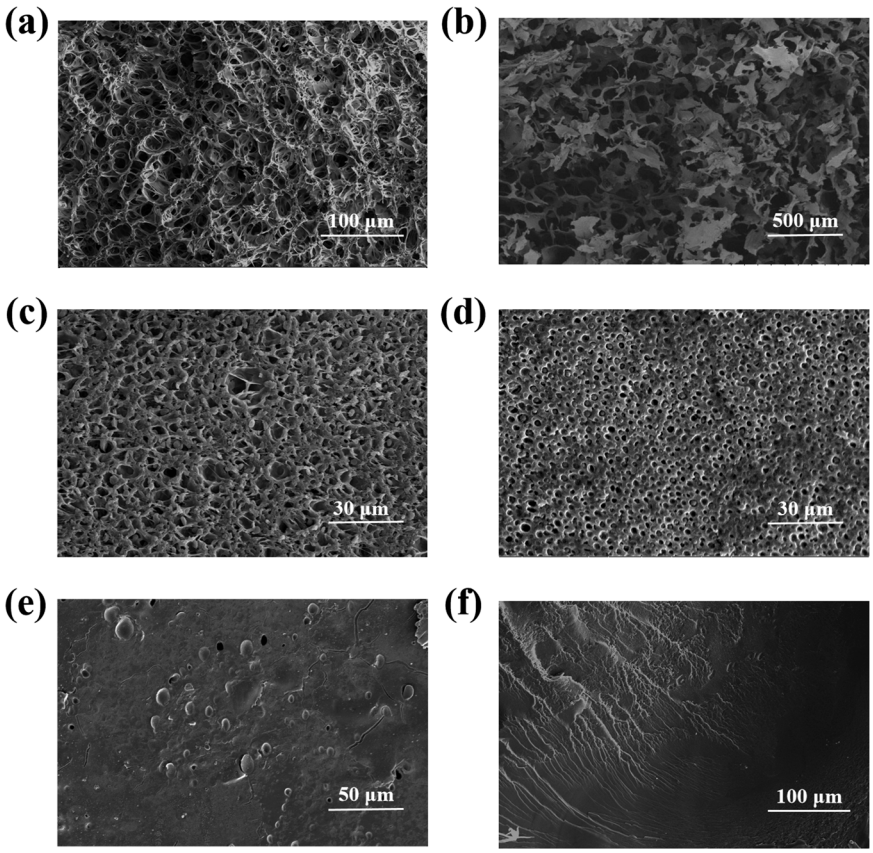

Fig. 3 Scanning electron micrographs of the (**a**) PAA/Al^{3+} hydrogel; (**b**) OSA/CMCS hydrogel; (**c**) H-1 hydrogel; (**d**) H-2 hydrogel; (**e**) H-3 hydrogel; (**f**) H-4 hydrogel

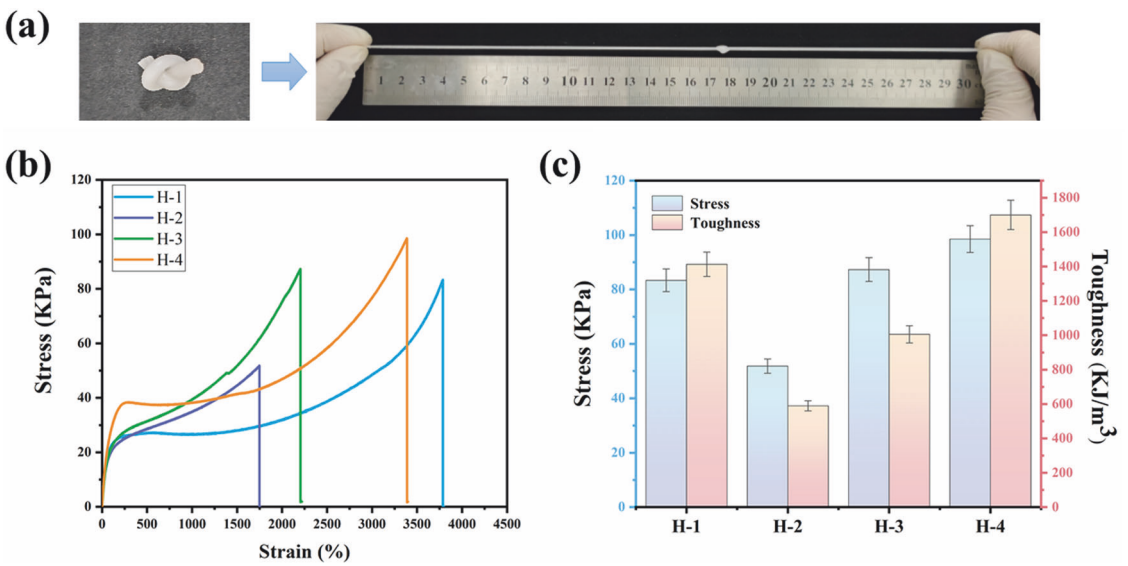

Fig. 4 **a** Tensile diagram of the PAA/CMCS/OSA/Al^{3+} hydrogel after knotting; (**b**, **c**) Tensile stress-strain diagram of the PAA/CMCS/OSA/Al^{3+} hydrogel and its corresponding maximum stress and toughness

hydrogels under 200% strain conditions. As shown in Fig. S2, in the first loading-unloading cycle, there is a significant hysteresis cycle with more energy dissipation, and this result indicates that the network structure of the hydrogel significantly changes during the stretching process. The energy loss of the PAA/CMCS/OSA/Al^{3+} hydrogel significantly decreased during the subsequent cycles, and this result indicates that the hydrogel had self-recovery properties. During the entire cycle, there was no time delay for the hydrogel to move to the next cycle, so the internal damage in the first cycle does not have sufficient time to recover; thus, the dissipated energy is always present throughout the loading-unloading cycle test.

Similarly, the PAA/CMCS/OSA/Al^{3+} hydrogels were tested under compression loading-unloading cycles at 50%, 60%, 70%, and 80% strain conditions, and their corresponding compressive stresses and dissipation energies were calculated. As shown in Fig. S3, both compressive stress and dissipated energy gradually increased with increasing strain. Figure S3 shows that PAA/CMCS/OSA/Al^{3+} did not fracture under large stresses, which is mainly attributed to its double network structure.

Analysis of self-healing properties of the PAA/CMCS/OSA/Al^{3+} hydrogel

The PAA/CMCS/OSA/Al^{3+} hydrogel exhibited excellent self-healing properties at room temperature. As shown in Fig. 5, the cylindrical hydrogel was truncated in the middle, and one section was stained and placed in contact with the other half for 20 min at room temperature. Then, the hydrogel was stretched such that the hydrogel healed well and regained its mechanical properties. To further observe the healing of the PAA/CMCS/OSA/Al^{3+} hydrogels, the healing sites of the H-1, H-3, and H-4 hydrogels were observed via electron microscopy, as shown in Fig. 5b. The truncated marks of the hydrogel were re-crosslinked together in a healed state under scanning electron microscopy.

To investigate the self-healing performance of the PAA/CMCS/OSA/Al^{3+} hydrogel, the tensile properties of the hydrogels before and after healing were compared. The above results indicate that H-1 and H-3 had better self-healing properties than H-2. The reason for this phenomenon may be that excess Al^{3+} disrupts the equilibrium of the hydrogel double network. As Fig. S4 shows, the tensile stress after self-healing in the PAA/CMCS/OSA/Al^{3+} hydrogel samples recovered to a maximum of 54% of the original tensile stress, and the toughness recovered to a maximum of 127% (H-3).

Rheological analysis of the PAA/CMCS/OSA/Al^{3+} hydrogel

In addition to the characterization of the self-healing properties of the PAA/CMCS/OSA/Al^{3+} in terms of macroscopic patterns and mechanical properties, dynamic oscillatory rheological tests were performed to quantify the self-healing properties of the hydrogels. As shown in Fig. 6, the energy storage modulus (G′) of this hydrogel was significantly greater than its loss modulus (G″) in the small strain range, which indicates that the hydrogel exhibited excellent solid-state elastic behavior in this range. When the strain increases, the energy storage modulus (G′) and loss

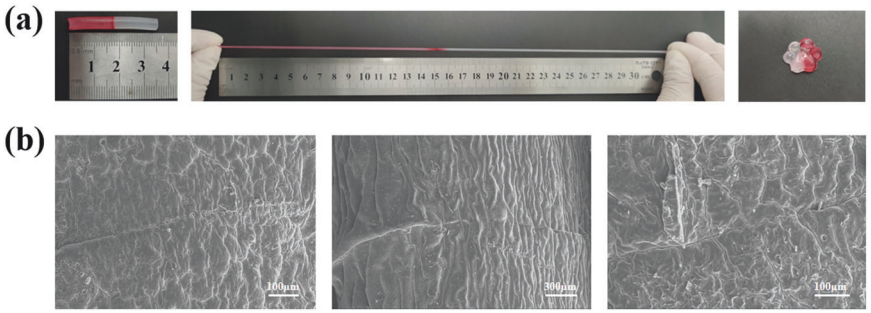

Fig. 5 **a** Self-healing pictures of the PAA/CMCS/OSA/Al^{3+} hydrogel under macroscopic conditions; **b** Healing under a scanning electron microscope

modulus (G″) intersect, which is usually considered a sign of gelation [35].

Then, we tested PAA/CMCS/OSA/Al^{3+} before and after self-healing at $\gamma = 1\%$ and $\gamma = 10\%$ strains, respectively, and Fig. 7 shows the test results. This result indicates that the double-crosslinked structure of H-1 reached a state of relative equilibrium. H-2 exhibited poor self-healing properties under large strains, and its self-healed energy storage modulus and loss modulus were unstable. This result indicates that more Al^{3+} disrupted the equilibrium cross-linked state of H-1, which is consistent with the mechanical stretching results. The energy storage modulus of H-3 increased after self-healing, but its loss modulus decreased, which indicates that the internal network of this hydrogel experienced limited healing after a short damage time, and the damaged network became weaker after a short connection time and was more likely damaged again. This result indicates that the imine bond structure in the PAA/CMCS/OSA/Al^{3+} hydrogel disrupts the cross-link equilibrium state at this time, and the network connection after self-healing of the hydrogel is poor when there are more CMCSs in the imine bond cross-link structure. The test results of H-4 show that H-4 has good self-healing properties. The hydrogel after self-healing had larger energy storage modulus and loss modulus than the original hydrogel under both high and low strains. This result indicates that H-4 regained a better cross-linked state at this ratio; therefore, its internal network was reconnected and more tightly connected after self-healing. The rheological test results demonstrate the self-healing performance of the PAA/CMCS/OSA/Al^{3+} hydrogel, which provides more possibilities for its application in practical scenarios.

Conductivity study of the PAA/CMCS/OSA/Al^{3+} hydrogel

The conductive properties of the PAA/CMCS/OSA/Al^{3+} hydrogel were characterized because some raw materials of the hydrogel have conductive properties. Figure 8a shows the conductivity of PAA/CMCS/OSA/Al^{3+}, which was 0.99 to −1.41 S/m. This result broadens the application of PAA/CMCS/OSA/Al^{3+} in real life. Furthermore, the relative

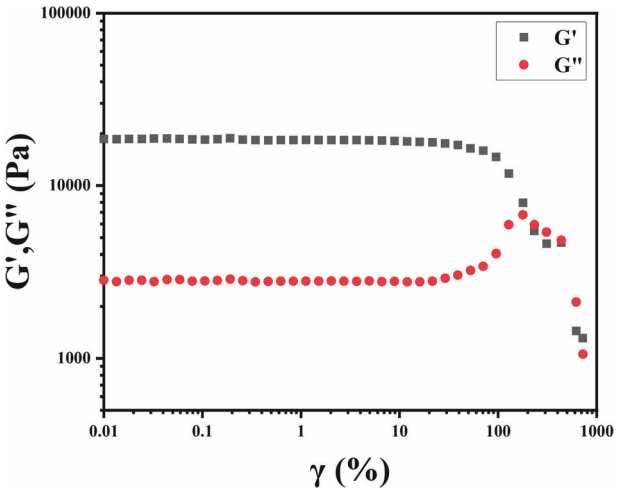

Fig. 6 Strain scan of the PAA/CMCS/OSA/Al^{3+} hydrogel (H-1)

resistance of the hydrogel was tested at different tensile strains. Figure 8b and c shows that the relative resistance of PAA/CMCS/OSA/Al^{3+} proportionally changes with the change in external strain, which indicates the high sensitivity of this hydrogel. Moreover, the corresponding relative resistance can be recovered when the strain returns to its original state. This excellent repeatable testing and sensing performance lays the foundation for combining this hydrogel with electrical signal sensing in practical scenarios.

Inspired by the good electrical conductivity of PAA/CMCS/OSA/Al^{3+}, we further characterized its self-healing properties via electrical signals. Figure 9 shows the conductivity of the original hydrogel, which gradually decreased, levelled off throughout the process, and finally stabilized at 1.40 S/m. The reason may be the short resting time of the hydrogel at the beginning, when the internal ions had not reached a relatively stable state. In addition, the gradual loss of water in the air for a long time can lead to the above results. Then, the hydrogel was truncated, and the healing process of the hydrogel was monitored after it contacted the two halves. The conductivity of the hydrogel significantly changed during the healing process after

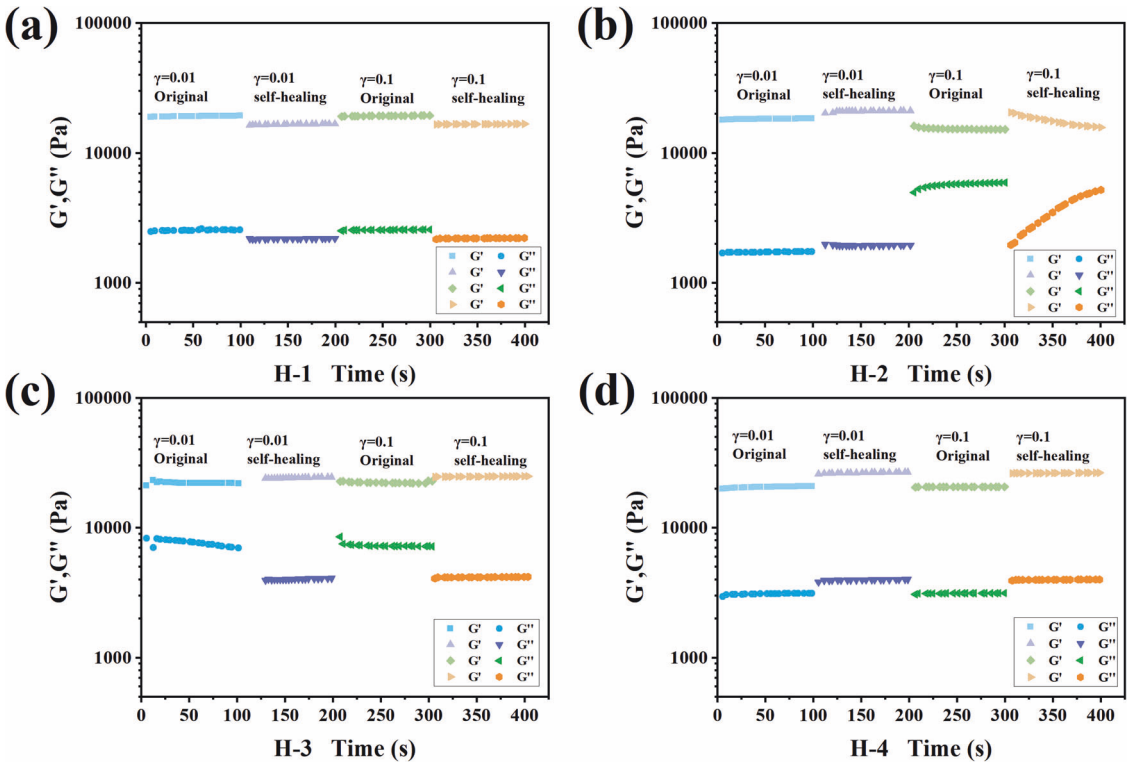

Fig. 7 Scanning test plots of the PAA/CMCS/OSA/Al^{3+} hydrogel before and after self-healing under different strains (**a**) H-1 (**b**) H-2 (**c**) H-3 (**d**) H-4

truncation. This method provides a new approach to characterize the self-healing properties of self-healing hydrogels with conductive properties.

Table 1 compares the mechanical properties, self-healing properties, and electrical conductivity of the PAA/CMCS/OSA/Al^{3+} hydrogel in this study with those of similar hydrogels, and these results further demonstrate the excellent overall performance of PAA/CMCS/OSA/Al^{3+}.

In vitro antibacterial performance analysis of the PAA/CMCS/OSA/Al^{3+} hydrogel

The antibacterial performance of the PAA/CMCS/OSA/Al^{3+} hydrogel was characterized by the inhibition circle method and plate counting method. As shown in Fig. 10, the hydrogel significantly inhibited both *E. coli* and *S. aureus* at a concentration of 10^7 CFU/mL. Because bacteria have negatively charged outer surfaces (due to the presence of lipopolysaccharide and/or phosphopeptide acid) [36], the PAA/CMCS/OSA/Al^{3+} hydrogel with positively charged substances can interact with bacteria and exhibit antibacterial properties. The results in Fig. 10 show that the PAA/CMCS/OSA/Al^{3+} hydrogel was more effective against *S. aureus*, and the hydrogel continued to inhibit *S. aureus* at a concentration of 10^8 CFU/mL after the test. The bacterial inhibitory effect of PAA/CMCS/OSA/Al^{3+} hydrogels is mainly due to the presence of Al^{3+}, CMCS, and OSA in the hydrogels [23, 37]. H-2 had a higher Al^{3+} content, so it had a slightly larger inhibition circle diameter in *S. aureus* than the other hydrogels. The H-3 hydrogel also showed better inhibition performance due to the higher CMCS content, and the aldehyde group in H-4 with a varying OSA content made H-4 exhibit antibacterial properties. Bacteria are divided into gram-positive and gram-negative bacteria according to their cell structure, and *S. aureus* and *E. coli* are typical examples of these two types of bacteria. Therefore, the difference in inhibition intensity of different hydrogel samples against the two bacteria may be due to the different structures of the bacteria and different degrees of binding and disruption of the antimicrobial substances with the bacterial structures [3, 38].

To confirm the antibacterial performance of the PAA/CMCS/OSA/Al^{3+} hydrogels, we tested the antibacterial performance of the hydrogels using the plate counting method. As shown in Fig. 11, the antibacterial effect of the hydrogel was more significant at lower bacterial concentrations with inhibition of up to 100% of the bacteria. To monitor bacterial growth in the presence of the hydrogel, a 12-h OD600 line graph of bacterial growth was generated, as shown in Fig. 12. The hydrogel began to inhibit the growth of bacteria mainly at the 2nd hour and maintained a stable inhibitory effect during the later co-cultivation, where the inhibitory effect was better for *S. aureus*, which is consistent with the results of the

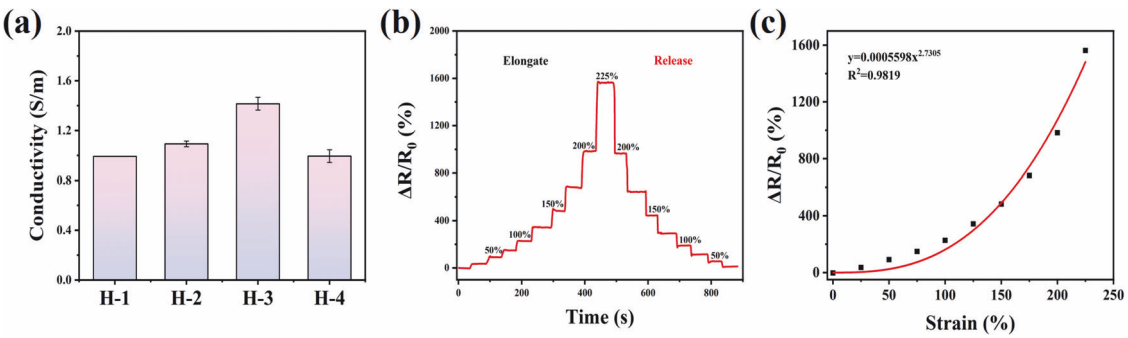

Fig. 8 **a** Electrical conductivity of the PAA/CMCS/OSA/Al^{3+} hydrogel; **b** relative resistance change in the PAA/CMCS/OSA/Al^{3+} hydrogel at different tensile strains; **c** fitted curve of $\Delta R/R_0$ versus strain

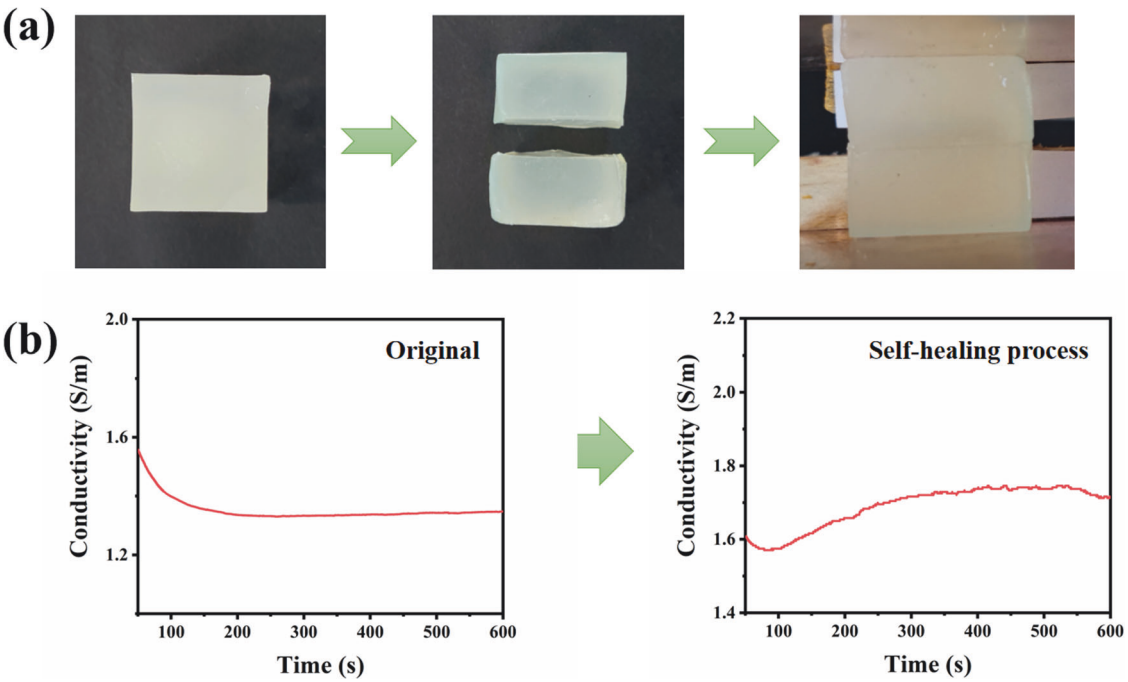

Fig. 9 Conductivity change monitoring process of PAA/CMCS/OSA/Al^{3+} hydrogel before and after self-healing (**a**) macroscopic state display before and after hydrogel self-healing (**b**) conductivity change curve corresponding to it

Table 1 Comparison of the performance of PAA/CMCS/OSA/Al^{3+} in this work and other reported self-healing antimicrobial hydrogels (N indicates not mentioned)

Materials	Tensile stress (KPa)	Tensile fracture strain (%)	Self-healing efficiency (%)	Electrical conductivity (S/m)	Ref
PAA/PPy-Fe	770	448	74.1 (Stress)	0.92	[39]
AA-Al^{3+}/OSA-AG	129.2	1125	75 (Stress) 55 (Strain)	0.085	[23]
PAA/PEI/AgPPy/Co^{2+}	16.8	~360	N	0.048	[40]
P(AM/AA/C_{18})-$ZnCl_2$	71	3280	35.2 (Strain)	1.4 ~ 2	[41]
PVA/PAA-PAM-IS/GC	840	784	95	0.6	[42]
PVA/gelatin/β-CD	26.4	1200	96	N	[43]
PAM/PBA-IL/CNF	369.5	1810	92	0.694	[44]
PAA/CMCS/OSA/Al^{3+}	98	3787	54 (Stress) 127 (Strain)	1.41	This work

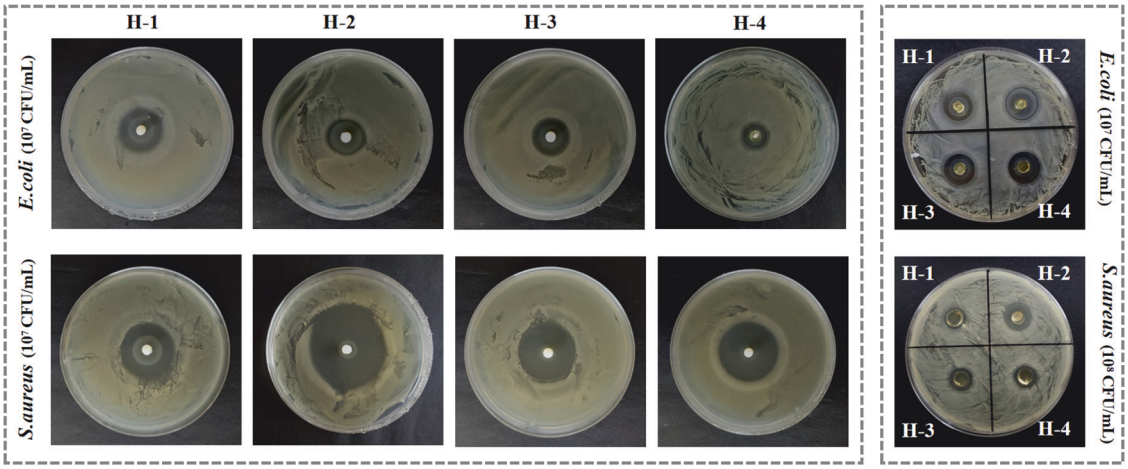

Fig. 10 Inhibition circle of the PAA/CMCS/OSA/Al^{3+} hydrogel

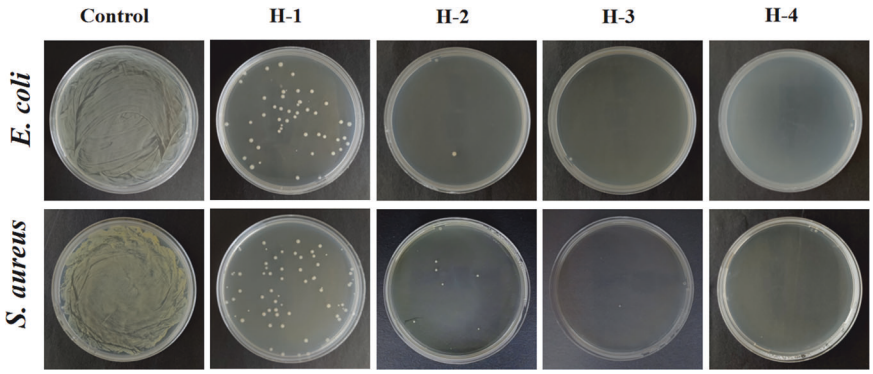

Fig. 11 In vitro antibacterial plate count picture of the PAA/CMCS/OSA/Al^{3+} hydrogel

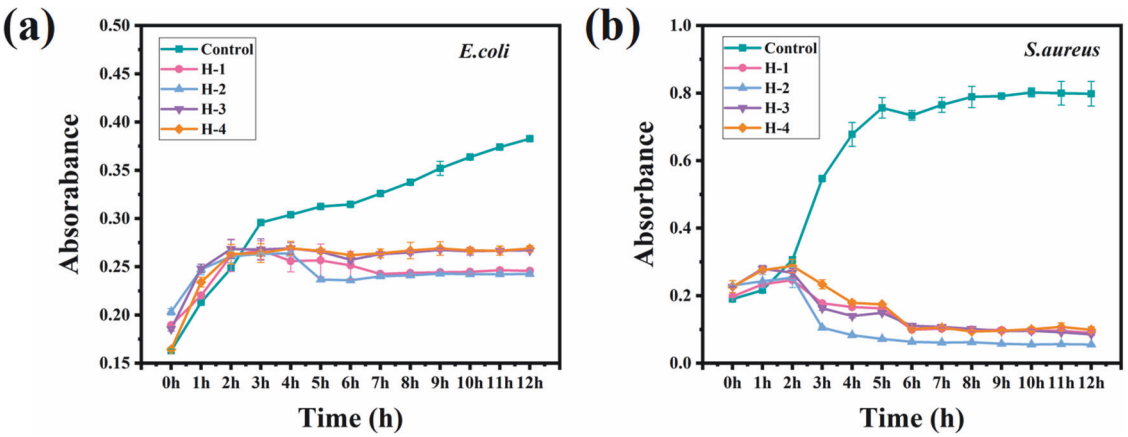

Fig. 12 Line graph of the inhibitory effect of PAA/CMCS/OSA/Al^{3+} hydrogel on the growth (12h) of (**a**) *E. coli* and (**b**) *S. aureus*

inhibition cycle. All test results show that the hydrogel has excellent antibacterial properties.

Conclusion

In this work, the hydrogel network formed by ligand bonding and hydrogel network formed by dynamic imine bonding were combined to form a double-network hydrogel. The ligand interaction was realized by acrylic acid (AA) with Al^{3+}, and the dynamic imine bonding network was realized by sodium-oxidized alginate (OSA) and carboxymethyl chitosan (CMCS). A PAA/CMCS/OSA/Al^{3+} hydrogel with excellent mechanical properties, self-healing properties, antibacterial properties, and electrical conductivity was prepared. The hydrogel has better

self-healing properties and better mechanical properties. Because there are substances with antimicrobial properties such as Al^{3+}, CMCS, and OSA in the hydrogel network, the hydrogel also better inhibited the growth of *E. coli* and *S. aureus*. In addition, the presence of Al^{3+} in this hydrogel network endows it with good electrical conductivity. The self-healing and antibacterial properties of this hydrogel lay the foundation for the application of hydrogels in biomedical applications, and its conductive properties provide ideas for hydrogels in smart sensing and signal monitoring.

Acknowledgements This work was supported by the National Natural Science Foundation of China (42076193) and the Ningbo Science and Technology Bureau (202002N3061).

Compliance with ethical standards

Conflict of interest The authors declare no competing interests.

References

1. Calvert P. Hydrogels for soft machines. Adv Mater. 2009;21:743–56. https://doi.org/10.1002/adma.200800534
2. Taylor DL, In Het Panhuis M. Self-healing hydrogels. Adv Mater. 2016;28:9060–93. https://doi.org/10.1002/adma.201601613
3. Li S, Dong S, Xu W, Tu S, Yan L, Zhao C, et al. Antibacterial hydrogels. Adv Sci (Weinh). 2018;5:1700527 https://doi.org/10.1002/advs.201700527
4. Tang L, Wu S, Qu J, Gong L, Tang J. A review of conductive hydrogel used in flexible strain sensor. Materials. 2020;13:3947. https://doi.org/10.3390/ma13183947
5. Li L, Scheiger JM, Levkin PA. Design and applications of photoresponsive hydrogels. Adv Mater. 2019;31:1807333.1–7. https://doi.org/10.1002/adma.201807333
6. Ma S, Yu B, Pei X, Zhou F. Structural hydrogels. Polymer. 2016;98:516–35. https://doi.org/10.1016/j.polymer.2016.06.053
7. Wang Y. Programmable hydrogels. Biomaterials. 2018;178:663–80. https://doi.org/10.1016/j.biomaterials.2018.03.008
8. Cheng W, Wu X, Zhang Y, Wu D, Meng L, Chen Y, et al. Recent applications of hydrogels in food safety sensing: Role of hydrogels. Trends Food Sci Technol. 2022;129:244–57. https://doi.org/10.1016/j.tifs.2022.10.004
9. Yao X, Liu J, Yang C, Yang X, Wei J, Xia Y, et al. Hydrogel paint. Adv Mater. 2019;31:1903062. https://doi.org/10.1002/adma.201903062
10. Khajouei S, Ravan H, Ebrahimi A. DNA hydrogel-empowered biosensing. Adv Colloid Interf Sci. 2020;275:102060. https://doi.org/10.1016/j.cis.2019.102060
11. Brumberg V, Astrelina T, Malivanova T, Samoilov A. Modern wound dressings: hydrogel dressings. Biomedicines. 2021;9:1235. https://doi.org/10.3390/biomedicines9091235
12. Li J, Mooney DJ. Designing hydrogels for controlled drug delivery. Nat Rev Mater. 2016;1:16071. https://doi.org/10.1038/natrevmats.2016.71
13. Guan X, Avci-Adali M, Alarcin E, Cheng H, Kashaf SS, Li Y, et al. Development of hydrogels for regenerative engineering. Biotechnol J. 2017;12:1600394. https://doi.org/10.1002/biot.201600394
14. Yang B, Song J, Jiang Y, Li M, Wei J, Qin J, et al. Injectable adhesive self-healing multicross-linked double-network hydrogel facilitates full-thickness skin wound healing. ACS Appl Mater Interfaces. 2020;12:57782–97. https://doi.org/10.1021/acsami.0c18948
15. He J, Zhang Z, Yang Y, Ren F, Li J, Zhu S, et al. Injectable self-healing adhesive ph-responsive hydrogels accelerate gastric hemostasis and wound healing. Nano-Micro Lett. 2021;13:80. https://doi.org/10.1007/s40820-020-00585-0
16. Chen J, He J, Yang Y, Qiao L, Hu J, Zhang J, et al. Antibacterial adhesive self-healing hydrogels to promote diabetic wound healing. Acta Biomaterialia. 2022;146:119–30. https://doi.org/10.1016/j.actbio.2022.04.041
17. Yang K, Zhou X, Li Z, Wang Z, Luo Y, Deng L, et al. Ultra-stretchable, self-healable, and tissue-adhesive hydrogel dressings involving nanoscale tannic acid/ferric ion complexes for combating bacterial infection and promoting wound healing. ACS Appl Mater Interfaces. 2022;14:43010–25. https://doi.org/10.1021/acsami.2c13283
18. Deng P, Yao L, Chen J, Tang Z, Zhou J. Chitosan-based hydrogels with injectable, self-healing and antibacterial properties for wound healing. Carbohydrate Polym. 2022;276. https://doi.org/10.1016/j.carbpol.2021.118718
19. Liu C, Xu Z, Chandrasekaran S, Liu Y, Wu M. Self-healing, antibacterial, and conductive double network hydrogel for strain sensors. Carbohydrate Polym. 2023;303. https://doi.org/10.1016/j.carbpol.2022.120468
20. Wang Z, Zhang X, Cao T, Wang T, Sun L, Wang K, et al. Antiliquid-interfering, antibacteria, and adhesive wearable strain sensor based on superhydrophobic and conductive composite hydrogel. ACS Appl. Mater. Interf. 2021;13:46022–32. https://doi.org/10.1021/acsami.1c15052
21. Wu L, Li L, Pan L, Wang H, Bin Y. MWCNTs reinforced conductive, self-healing polyvinyl alcohol/carboxymethyl chitosan/oxidized sodium alginate hydrogel as the strain sensor. J Appl Polym Sci. 2021;138. https://doi.org/10.1002/app.49800
22. Chen J, Li S, Zhang Y, Wang W, Zhang X, Zhao Y, et al. A reloadable self-healing hydrogel enabling diffusive transport of c-dots across gel-gel interface for scavenging reactive oxygen species. Adv. Healthcare Mater. 2017;1700746. https://doi.org/10.1002/adhm.201700746
23. Zhao L, Ke T, Ling Q, Liu J, Li Z, Gu H. Multifunctional ionic conductive double-network hydrogel as a long-term flexible strain sensor. ACS Appl Polym Mater. 2021;3:5494–508. https://doi.org/10.1021/acsapm.1c00805
24. Pan J, Jin Y, Lai S, Shi L, Fan W, Shen Y. An antibacterial hydrogel with desirable mechanical, self-healing and recyclable properties based on triple-physical crosslinking. Chem Eng J. 2019;370:1228–38. https://doi.org/10.1016/j.cej.2019.04.001
25. Ma Y, Yao J, Liu Q, Han T, Zhao J, Ma X, et al. Liquid bandage harvests robust adhesive, hemostatic, and antibacterial performances as a first-aid tissue adhesive. Adv Funct Mater. 2020;30. https://doi.org/10.1002/adfm.202001820
26. Wang H, Chen X, Wen Y, Li D, Sun X, Liu Z, et al. A study on the correlation between the oxidation degree of oxidized sodium alginate on its degradability and gelation. Polymers. 2022;14:1679. https://doi.org/10.3390/polym14091679
27. Gomez CG, Rinaudo M, Villar MA. Oxidation of sodium alginate and characterization of the oxidized derivatives. Carbohydr Polym. 2007;67:296–304. https://doi.org/10.1016/j.carbpol.2006.05.025
28. Anjum S, Gurave P, Badiger MV, Torris A, Tiwari N, Gupta B. Design and development of trivalent aluminum ions induced self-healing polyacrylic acid novel hydrogels. Polymer. 2017;126:196–205. https://doi.org/10.1016/j.polymer.2017.08.045
29. Klosinski KK, Wach RA, Girek-Bak MK, Rokita B, Kolat D, Kaluzinska-Kolat Z, et al. Biocompatibility and mechanical

properties of carboxymethyl chitosan hydrogels. Polymers. 2022;15:144. https://doi.org/10.3390/polym15010144
30. Cao J, Wu P, Cheng Q, He C, Chen Y, Zhou J. Ultrafast fabrication of self-healing and injectable carboxymethyl chitosan hydrogel dressing for wound healing. ACS Appl Mater Interfaces. 2021;13:24095–105. https://doi.org/10.1021/acsami.1c02089
31. Zhao X, Wu H, Guo B, Dong R, Qiu Y, Ma PX. Antibacterial anti-oxidant electroactive injectable hydrogel as self-healing wound dressing with hemostasis and adhesiveness for cutaneous wound healing. Biomaterials. 2017;122:34–47. https://doi.org/10.1016/j.biomaterials.2017.01.011
32. Gupta B, Tummalapalli M, Deopura BL, Alam MS. Preparation and characterization of in-situ crosslinked pectin-gelatin hydrogels. Carbohydr Polym. 2014;106:312–8. https://doi.org/10.1016/j.carbpol.2014.02.019
33. Li T, Hu X, Zhang Q, Zhao Y, Wang P, Wang X, et al. Poly(acrylic acid)-chitosan @ tannic acid double-network self-healing hydrogel based on ionic coordination. Polym Adv Technol. 2020;31:1648–60. https://doi.org/10.1002/pat.4893
34. Wei Z, Yang JH, Liu ZQ, Xu F, Zhou JX, Zrínyi M, et al. Novel biocompatible polysaccharide-based self-healing hydrogel. Adv Funct Mater. 2015;25:1352–9. https://doi.org/10.1002/adfm.201401502
35. Shin M, Shin S-H, Lee M, Kim HJ, Jeong JH, Choi YH, et al. Rheological criteria for distinguishing self-healing and non-self-healing hydrogels. Polymer 2021;229. https://doi.org/10.1016/j.polymer.2021.123969
36. Bolatchiev A. Antibacterial activity of human defensins against Staphylococcus aureus and Escherichia coli. PeerJ. 2020;8. https://doi.org/10.7717/peerj.10455
37. Marin L, Ailincai D, Mares M, Paslaru E, Cristea M, Nica V, et al. Imino-chitosan biopolymeric films. Obtaining, self-assembling, surface and antimicrobial properties. Carbohydr Polym. 2015;117:762–70. https://doi.org/10.1016/j.carbpol.2014.10.050
38. Cao Z, Luo Y, Li Z, Tan L, Liu X, Li C, et al. Macromol Biosci. Macromol Biosci. 2021;21:e2000252. https://doi.org/10.1002/mabi.202000252
39. Ginting M, Pasaribu SP, Masmur I, Kaban J, Hestina. Self-healing composite hydrogel with antibacterial and reversible restorability conductive properties. Rsc Adv. 2020;10:5050–7. https://doi.org/10.1039/d0ra00089b
40. Lin Z, Fan D, Li G, He L, Qin X, Zhao B, et al. Antibacterial, adhesive, and conductive hydrogel for diabetic wound healing. Macromol Biosci. 2023;23. https://doi.org/10.1002/mabi.202200349
41. Zhao X, Wang H, Luo J, Ren G, Wang J, Chen Y, et al. Ultra-stretchable, adhesive, anti-freezing, conductive, and self-healing hydrogel for wearable devices. Acs Appl Polym Mater. 2022;4:1784–93. https://doi.org/10.1021/acsapm.1c01618
42. Min J, Zhou Z, Zheng J, Yan C, Sha H, Hong M, et al. Self-healing, water-retaining, antifreeze, conductive PVA/PAA-PAM-IS/GC composite hydrogels for strain and temperature sensors. Macromol Mater Eng. 2022;307. https://doi.org/10.1002/mame.202100948
43. Fan X, Geng J, Wang Y, Gu H, PVA/gelatin/beta-CD-based rapid self-healing supramolecular dual-network conductive hydrogel as bidirectional strain sensor. Polymer. 2022;246. https://doi.org/10.1016/j.polymer.2022.124769
44. Yao X, Zhang S, Qian L, Wei N, Nica V, Coseri S, et al. Super stretchable, self-healing, adhesive ionic conductive hydrogels based on tailor-made ionic liquid for high-performance strain sensors. Adv Funct Mater. 2022;32. https://doi.org/10.1002/adfm.202204565